Biochimica et Biophysica Acta 1838 (2014) 2939–2946

Contents lists available at ScienceDirect

Biochimica et Biophysica Acta

journal homepage: www.elsevier.com/locate/bbamem

Labeling phospholipid membranes with lipid mimetic luminescent metal complexes

Adam Mechler *, Bradley D. Stringer, Muhammad S.H. Mubin, Egan H. Doeven, Nicholas W. Phillips, Jesse Rudd-Schmidt, Conor F. Hogan

Department of Chemistry, La Trobe Institute for Molecular Science, La Trobe University, VIC 3086, Australia

ARTICLE INFO

Article history:
Received 7 May 2014
Received in revised form 31 July 2014
Accepted 5 August 2014
Available online 12 August 2014

Keywords:
Fluorescence microscopy
Lipid membrane
Biomimetics
Luminescent metal complex
SAXS

ABSTRACT

Lipid-mimetic metallosurfactant based luminophores are promising candidates for labeling phospholipid membranes without altering their biophysical characteristics. The metallosurfactants studied exhibit high structural and physicochemical similarity to phospholipid molecules, designed to incorporate into the membrane structure without the need for covalent attachment to a lipid molecule. In this work, two lipid-mimetic phosphorescent metal complexes are described: $[Ru(bpy)_2(dn\text{-}bpy)]^{2+}$ and $[Ir(ppy)_2(dn\text{-}bpy)]^{+}$ where bpy is 2,2′-bipyridine, dn-bpy is 4,4′-dinonyl-2,2′-bipyridine and ppy is 2-phenylpyridine. Apart from being lipid-mimetic in size, shape and physical properties, both complexes exhibit intense photoluminescence and enhanced photostability compared with conventional organic fluorophores, allowing for prolonged observation. Moreover, the large Stokes shift and long luminescence lifetime associated with these complexes make them more suitable for spectroscopic studies. The complexes are easily incorporated into dimyristoil-phosphatidyl-choline (DMPC) liposomes by mixing in the organic solvent phase. DLS reveals the labeled membranes form liposomes of similar size to that of neat DMPC membrane. Synchrotron Small-Angle X-ray Scattering (SAXS) measurements confirmed that up to 5% of either complex could be incorporated into DMPC membranes without producing any structural changes in the membrane. Fluorescence microscopy reveals that 0.5% label content is sufficient for imaging. Atomic Force Microscopic imaging confirms that liposomes of the labeled bilayers on a mica surface can fuse into a flat lamellar membrane that is morphologically identical to neat lipid membranes. These results demonstrate the potential of such lipid-mimetic luminescent metal complexes as a new class of labels for imaging lipid membranes.

1. Introduction

Imaging and spectroscopic characterization methods based on fluorescent labeling of biomolecules, such as confocal imaging, Förster resonance energy transfer (FRET) and fluorescence recovery after photobleaching (FRAP) are performed routinely in biophysical membrane studies [1]. The majority of fluorescent probes used in these studies is based on fused aromatic or heterocyclic rings [2] such as anthracene [3,4], fluorene [5] and pyrene [6,7]. These probes are typically characterized by high quantum yields, small Stokes shifts, short luminescence lifetimes, and often high susceptibility to photobleaching [8]. While a short luminescent lifetime and photochemical instability might occasionally be advantageous, many applications such as super resolution microscopy demand longer luminescent lifetimes, increased photostability and a larger Stokes shift [8–11].

Beyond the shortcomings in their photophysical properties, in the context of membrane labeling, planar heterocyclic luminophores also suffer from unfavorable molecular geometries. Lipid membranes are dynamic self-assembled systems, where any small change in the constituents can alter the balance of the second order interactions that stabilize the bilayer, affecting its physical properties [12,13]. For example, the effect of cholesterol on biophysical properties such as lipid mobility and membrane thickness is well documented [14]. Cholesterol is a weakly amphiphilic planar fused heterocyclic molecule. Consistently, the incorporation of other large fused heterocycles such as organic fluorophores has a similar effect [15–20]: it can change the membrane phase transition temperature [16], decrease the acyl chain order and inhibit lateral diffusion [17], increase inter-bilayer lipid transfer [19] and can even lead to loss of membrane integrity [20]. Some labels are less intrusive, however even subtle changes in lamellar thickness, surface tension and bending rigidity affect the stable morphologies of the membrane, such as its ability to form liposomes or to fuse into

Abbreviations: AFM, atomic force microscopy; DLS, dynamic light scattering; DMPC, 1,2-ditetradecanoyl-sn-glycero-3-phosphocholine

* Corresponding author.
E-mail address: a.mechler@latrobe.edu.au (A. Mechler).

http://dx.doi.org/10.1016/j.bbamem.2014.08.005
0005-2736/

supported bilayers on surfaces [13]. Accordingly, novel approaches to labeling membranes in a biomimetic manner are required.

Transition metal complexes such as those based on Ru(II) and Ir(III) fulfill photophysical requirements and can be easily tailored synthetically to possess desired structural attributes. These complexes display molecular photoluminescence from a metal-to-ligand and/or intraligand charge transfer excited state and relaxation occurs via a partially forbidden transition, so excited state lifetimes are often relatively long (10 ns–10 μs) [21–23]. The complexes also exhibit large Stokes shifts (up to few hundred nanometers) [8]; enhanced photostability as well as comparable and sometimes higher quantum yield than organic fluorophores [24,25]. While there has been a recent increase in reports of using metal coordination complex labels in cell biology [9,26–29], relatively few such probes have been proposed for phospholipid membrane studies. Ruthenium complexes that anchor to bilayers by a thioether-cholestanol hybrid ligand [30], dipyridophenazine–ruthenium complexes that "float" in the bilayer [31], as well as lipophilic Ir(III) polypyridine complexes with pendant alkyl chains of 2, 10 and 18 carbons [32] have been proposed as membrane probes. However, these probes do not imitate the geometry and fundamental physical properties of the phospholipids closely enough. As a solution, head group modification of lipids was proposed, such as coupling a luminescent Ru(II) complex to the amino group of phosphatidyl ethanolamine which was used to study membrane motion on a nanosecond timescale [33,34]. An alternative and easier strategy is to use metallosurfactants that have been developed to create neat micellar systems and/or to create micellar mixtures with simple surfactants [35,36]. There is no information, however, on the physical properties of phospholipid membranes labeled with metallosurfactant luminophores.

Here, the use of two lipid-mimetic metallosurfactants, based on well-known structural motifs of luminescent iridium and ruthenium complexes, is proposed for this purpose: $[Ru(bpy)_2(dn\text{-}bpy)]^{2+}$ and $[Ir(ppy)_2(dn\text{-}bpy)]^{+}$ where bpy is 2,2′-bipyridine, dn-bpy is 4,4′-dinonyl-2,2′-bipyridine and ppy is 2-phenylpyridine. Our results suggest that the use of these metallosurfactants as lipid-mimetic labels has only negligible effect on the membrane properties, while offering significant photophysical advantages over traditional fluorophores.

2. Materials and methods

2.1. Materials

1,2-Ditetradecanoyl-sn-glycero-3-phosphocholine (dimyristoil-phosphatidyl-choline, DMPC) 1,2-ditetradecanoyl-sn-glycero-3-phosphoglycerol (dimyristoil-phosphatidyl-glycerol, DMPG) and cholesterol were purchased from Avanti Polar Lipids (Alabaster, AL, USA). Chloroform (ACS Reagent, ≥99.8%) was purchased from Sigma–Aldrich (Castle Hill, NSW, Australia). Lipid mimetic metal complexes; the precursors used for synthesis of the complexes 4,4′-dinonyl-2,2′-dipyridyl and bis(2,2′-bipyridine)dichlororuthenium(II) hydrate were purchased from Sigma Aldrich (>99%), and used without further purification. Sodium chloride (Ultra, ≥99.5% (AT)), potassium phosphate monobasic (ACS reagent, ≥99%), and potassium phosphate dibasic (ACS reagent, ≥99%) were purchased from Sigma–Aldrich (Castle Hill, NSW, Australia). Ultrapure water with a resistivity of 18.2 MΩ-cm was used (Milli-Q). Dry CH_3CN for analytical purposes was distilled from CaH_2 under nitrogen.

2.2. Synthesis

The molecular structure of the complexes is shown in Fig. 1. It should be noted that the actual three dimensional equidistant alignment of the ligands around the central metal leads to a spherical "head group" with two parallel alkane chains.

$[Ru(bpy)_2(dn\text{-}bpy)][PF_6]_2$: The ruthenium complex was synthesized using a small variation on a well-established method [37,38]. Briefly, 80 mg bis(2,2′-bipyridine)dichlororuthenium(II) hydrate (0.165 mmol) and 77.6 mg 4,4′-dinonyl-2,2′-dipyridyl (0.189 mmol, 15% excess) were dissolved in 75 mL 90:10 methanol:water under N_2 atmosphere. The mixture was heated and refluxed for 5 h, a color change from dark purple to dark red was observed. The solvent was removed via rotary evaporation, and the residue was dissolved in acetone. Saturated potassium hexafluorophosphate solution was added in excess, causing precipitation of the crude hexafluorophosphate complex salt. The crude complex was recrystallized from acetone/water and dried for a final yield of 82%.

$[Ir(ppy)_2(dn\text{-}bpy)][PF_6]$:$[Ir(ppy)_2(dn\text{-}bpy)]^{+}$ was synthesized by a well-established method [39] from the iridium dichloro-bridged dimer, tetrakis(2-phenylpyridine-C [2],N′)(μ-dichloro) diiridium–$[Ir(ppy)_2Cl]_2$, which was synthesized using the method of Sprouse et al. [40] 100 mg iridium dichloro-bridged dimer (0.093 mmol) and 80 mg 4,4′-dinonyl-2,2′-dipyridyl (0.196 mmol, 5% excess) were dissolved in 40 mL N_2 purged dichloromethane. The solution was refluxed under N_2 atmosphere for 24 h. The solvent was removed via rotary evaporation, and the residue was dissolved in the minimum amount of acetone. Saturated KPF_6 was added in excess, causing a bright yellow solid to precipitate. This solid was washed sparingly with cold ether, and finally purified on a sephadex LH-20 column using acetonitrile mobile phase. The bright yellow luminescent (UV, 365 nm) band was collected and the solvent was removed; the collected solid was dried for a final yield of 85%.

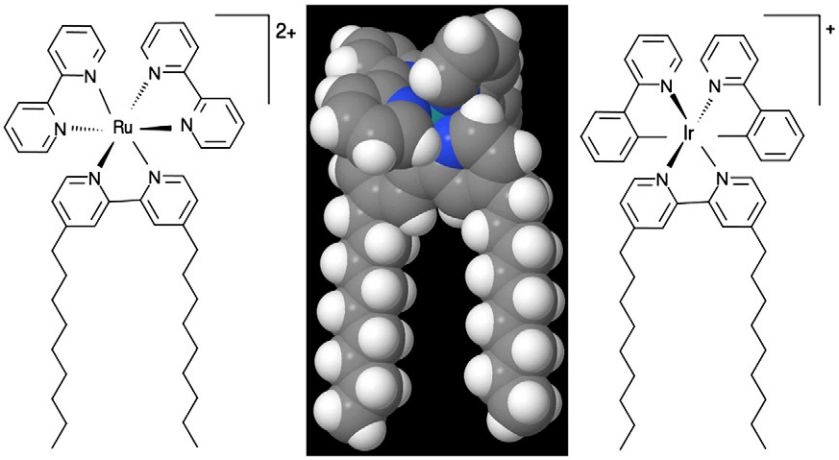

Fig. 1. Schematic molecular structure (left) and space filling model (middle) of $[Ru(bpy)_2(dn\text{-}bpy)]^{2+}$; molecular structure of $[Ir(ppy)_2(dn\text{-}bpy)]^{+}$ (right).

Photophysical measurements: The absorbance characteristics of the $[Ru(bpy)_2(dn\text{-}bpy)]^{2+}$ and $[Ir(ppy)_2(dn\text{-}bpy)]^{+}$ complexes were investigated using a Cary UV–Vis spectrophotometer (Agilent), while emission spectra, quantum yields and lifetimes of the metal complexes were measured using a Nanolog (HORIBA Jobin Yvon IBH) spectrometer. Emission spectra were recorded using an excitation wavelength of either 350 nm (Iridium) or 450 nm (Ruthenium) of 3 μM solutions in acetonitrile or incorporated into the liposomes in PBS. Emission spectra were corrected for variations in source intensity, gratings and detector response with wavelength.

The photoluminescence quantum yields of the two complexes, both in acetonitrile and incorporated into the liposomes dispersed in PBS, were acquired at room temperature (22 ± 2 °C) using a Quanta-phi HORIBA Scientific 6 in. diameter integrating sphere connected to the Nanolog via optical fiber bundles. Deoxygenated solutions were prepared in a nitrogen free glovebox with acetonitrile purged of oxygen by three freeze/pump/thawing cycles. Absolute quantum yields were calculated by the four-plot method using Fluoressence v3.5 software using the equation;

$$\phi_p = \frac{\text{Photons Out}}{\text{Photons In}} = \frac{(E_c - E_a)/A}{L_a - L_c}$$

where E_c is the integrated luminescence of the sample, E_a is the integrated luminescence of the blank, A is the area factor due to CCD integration time, L_a is the integrated excitation from the blank and L_c is the integrated excitation from the sample.

Excited state lifetimes in solutions and in the liposome dispersions were measured using time correlated single photon counting (TCSPC) and correlated by a time-to-amplitude converter (TAC) in forward TAC mode. Nanoled 340 (344 nm) and Nanoled 460 (451 nm) lasers were pulsed at 100 kHz. The emission decay was monitored at the maxima of the emission spectra and the band width set to 10 nm. Signals were collected using a FluoroHub counter and the data analyzed using DAS6 software (HORIBA Jobin Yvon IBH).

2.3. Incorporation of $[Ru(bpy)_2(dn\text{-}bpy)]^{2+}$ and $[Ir(ppy)_2(dn\text{-}bpy)]^{+}$ into phospholipid membranes and preparation of liposomes

The metal complexes were mixed in chloroform solution with neat DMPC, DMPC:DMPG 4:1 and DMPC:cholesterol 9:1 lipid mixtures at 0.1–5 mol% concentrations and aliquoted into glass test tubes. The solvent was then evaporated under a gentle stream of N_2 and desiccated overnight to form dry thin films of metal complex incorporated lipids. These dry films were re-suspended in aqueous buffer (20 mM phosphate buffered saline containing 100 mM NaCl at pH 6.7) with slow maceration at 37 °C, and then vortexed for 1 min and briefly sonicated (~30 s.) before use, to yield suspensions with 1 mM lipid concentration. This suspension was further diluted ~10× for membrane deposition. To confirm the presence of liposomes a Malvern Zetasizer dynamic light scattering instrument was used; measurements were performed at 25 °C.

Importantly, this sample preparation method yields multiwall liposomes (MLVs) that are required for SAXS measurements; however the broad size distribution of spontaneously forming liposomes is also suitable for bilayer fusion as it has been demonstrated before [47], as well as for fluorescence microscope imaging that requires large liposomes. The ability to use the same liposome preparation method for all measurements is a major advantage for the comparability of the results between the different methods.

2.4. Microscopy

Microscopic imaging was conducted using a Nikon TS 100 epifluorescence microscope with a UV lamp excitation source and a Leica TCS SP2 laser scanning confocal fluorescence microscope with a blue laser. Imaging was done in solution, using a thin (~1 mm) cuvette, with Nikon oil immersion objectives. Non-confocal images were cleared of diffraction using an unsharp masking method. AFM experiments were performed using an NT-MDT Ntegra AFM in intermittent contact mode, with NT-MDT NSG01 backside gold coated probes (length: 125 μm, nominal resonant frequency 87–230 kHz, typical apex radius 10 nm). The noise limited resolution of this system is ~0.1 nm and it is routinely used for high-resolution imaging of biomolecular systems [47,50]. Samples for AFM measurements have been prepared by pipetting 10 μl of liposome suspension to freshly cleaved mica surface, diluted with 20 μl buffer and then incubated for 15 min at 37 °C, a process that leads to full bilayer fusion for DMPC lipids [47]; samples were then carefully rinsed with drops of ultrapure water to remove excess solution and salts, and dried under a stream of nitrogen gas.

2.5. Small angle X-ray scattering measurement

X-ray diffraction patterns were recorded at the Australian Synchrotron SAXS/WAXS beamline using a hybrid pixel detector (PILATUS). $\lambda = 0.1033$ nm wavelength was used and the scattering curves were in a q-range from 0.2 to 11 nm^{-1} at photon energy 12 keV. For all SAXS experiments 5 mol% label content was used. The samples were inserted into 1.0 mm quartz capillaries and measured in flow using a syringe pump. The background correction was performed by measuring the scattering of a capillary tube filled with PBS in 100 mM NaCl and subtracting from the scattering of the samples. Exposure time was typically 10 s. Experiments were performed at 25 °C that is above the phase transition temperature of DMPC to allow for the relaxation of interlamellar strain. Data processing was carried out using SAXS15ID and Origin 7.0 (www.originlab.com) softwares.

3. Results and discussion

3.1. Photophysical properties

The photophysical properties of $[Ru(bpy)_2(dnbpy)]^{2+}$ are expected to be similar to $[Ru(bpy)_3]^{2+}$ [42]. Therefore, the large UV absorption peak at ~285 nm (Fig. 2A) is assigned to a ligand centered (LC) $\pi \rightarrow \pi^*$ transition while the absorption in the visible region at about 450 nm, is due to a $d \rightarrow \pi^*$ metal to ligand charge transfer (MLCT) transition [42]. Following optical excitation, the initially produced singlet ^{1}MLCT state decays rapidly through intersystem crossing to the corresponding triplet state (^{3}MLCT) with close to unit efficiency. De-excitation of this triplet state results in an intense luminescence centered at 628 nm in acetonitrile, which is red-shifted to 655 nm when the $[Ru(bpy)_2(dnbpy)]^{2+}$ complex is incorporated in the liposomes, as shown in Fig. 2B. The sensitivity of the emission wavelength to medium is characteristic of charge transfer excited states where excitation may be accompanied by significant changes in dipole moment. Similar to previously reported bis-cyclometallated iridium complexes, $[Ir(ppy)_2(dnbpy)]^{+}$ exhibits intense absorption in the UV associated with its ligands (LC $\pi \rightarrow \pi^*$, 250 nm), and quite low intensity MLCT bands in the visible ($d \rightarrow \pi^*$ at 290–480 nm). Similar to the ruthenium complex, the emission is red-shifted from 586 nm when $[Ir(ppy)_2(dnbpy)]^{+}$ is dissolved in acetonitrile, to 600 nm when incorporated in the liposomes. Again, the emission originates from a triplet excited state. However, in this case the excited state likely contains significant intra-ligand (i.e. LLCT) as well as MLCT character [39]. This observation is consistent with the relatively lower sensitivity of the emission maximum to environment compared with the ruthenium complex which is a pure MLCT emitter. Both complexes exhibit large Stokes shifts in excess of 100 nm, characteristic of inorganic fluorophores of this type. The complexes are remarkably photostable, neither storage in ambient light or prolonged exposure to UV (e.g. during fluorescence microscopy imaging) caused appreciable loss of intensity.

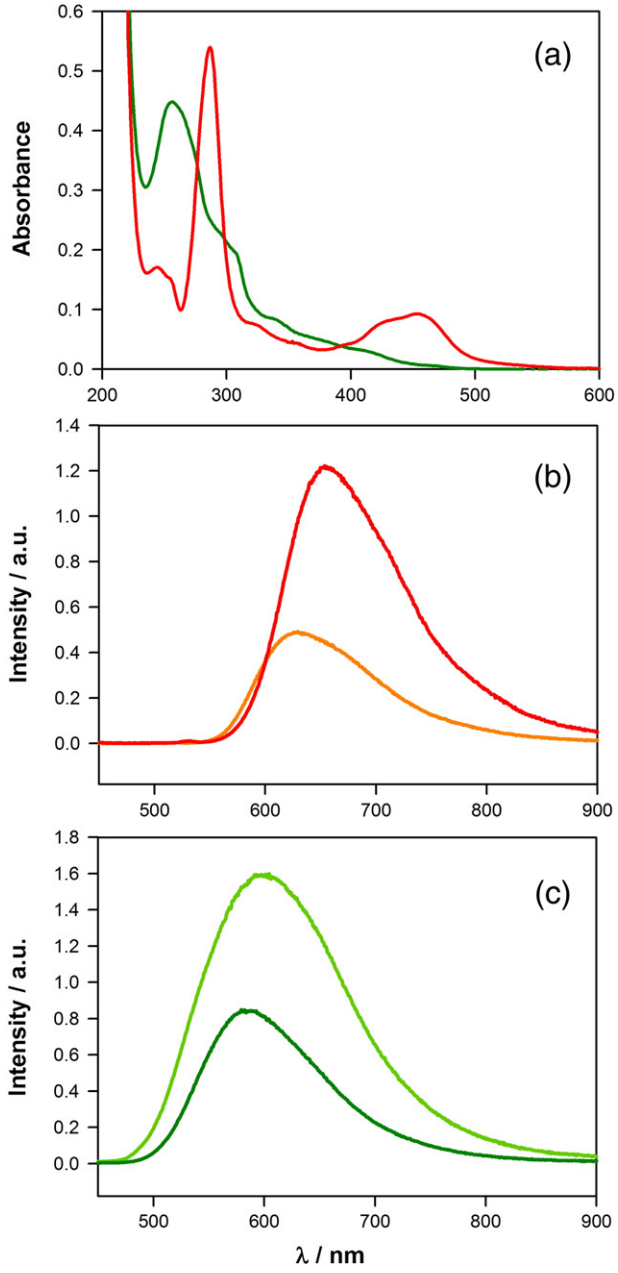

Fig. 2. (a) Absorbance spectra of $[Ru(bpy)_2(dn\text{-}bpy)]^{2+}$ (red) and $[Ir(ppy)_2(dn\text{-}bpy)]^{+}$ (green) in acetonitrile. (b) Photoluminescence spectra of the ruthenium complex in aerated acetonitrile solution (orange) and in liposomes (red). (c) Photoluminescence spectra of the iridium complex in aerated acetonitrile solution (dark green) and in liposomes (light green). Each solution is 3 μM in concentration. Emission intensities have been normalized according to the absorbance of each sample at the wavelength of excitation.

As shown by the data in Table 1, the photoluminescence quantum yields of the complexes in deaerated acetonitrile were determined to be 6.4% and 23.1% for $[Ru(bpy)_2(dnbpy)]^{2+}$ and $[Ir(ppy)_2(dnbpy)]^{+}$ respectively, similar to the quantum yields of $[Ru(bpy)_3]^{2+}$ and comparable iridium complexes [41]. In aerated solutions these quantum yields decreased to 0.9% and 2.6% respectively due to the well-known sensitivity of triplet excited states to oxygen quenching. When incorporated into the liposomes however, the quantum yields in aerated medium increase to 2.7% and 8.4% for the iridium and ruthenium complex respectively, suggesting that the liposome environment provides partial protection from oxygen quenching.

In order to gain further insight into the photophysical properties of the complexes and the effect of the liposome environment on these properties, lifetimes of the excited states were characterized (see Table 1 and Fig. S1). The lifetime of $[Ru(bpy)_2(dnbpy)]^{2+*}$ in oxygen-free acetonitrile solution was 888 ns. This decreased to 147 ns in aerated acetonitrile but increased to 368 ns when the complex was incorporated into liposomes. Similarly, for $[Ir(ppy)_2(dnbpy)]^{+*}$, the lifetime in deaerated solution was 555 ns, decreasing to 63 ns in aerated solution acetonitrile with again a partial recovery when incorporated into the liposome. In this case however, a multi-exponential decay was observed, which could be fitted by three lifetimes; 610 ns, 161 ns and 70 ns (161 ns being the dominant component). This behavior is consistent with the fact that the iridium complex may occupy one of three micro-environments within a multiwall liposome: the external leaflet exposed to the bulk of the solvent, the internal leaflet exposed to the encapsulated solvent, or in one of the intermittent leaflets of a multilayer structure that is not exposed to the solvent. This effect is prominent with the iridium complex because it has a greater sensitivity to oxygen quenching. Thus the lifetime of the excited state of the iridium complex might be used to probe the local lipid environment.

3.2. Biophysical characterization

$[Ru(bpy)_2(dn\text{-}bpy)]^{2+}$ and $[Ir(ppy)_2(dnbpy)]^{+}$ readily incorporated into neat DMPC, DMPC:DMPG 4:1 and DMPC:cholesterol 9:1 lipid mixtures at concentrations ranging from 0.1% to 5%, yielding liposomes of observable size. Using wide field and confocal fluorescence microscopy to image the labeled liposomes, it was found that as low as 0.5 mol% of $[Ru(bpy)_2(dn\text{-}bpy)]^{2+}$ or $[Ir(ppy)_2(dnbpy)]^{+}$ provided sufficient luminescent intensity for imaging in aqueous medium (Fig. 3: neat DMPC; Fig. S2: DMPC:DMPG 4:1; Fig. S3: DMPC:cholesterol 9:1). The images were taken in a cuvette, to avoid confinement induced fusion between a coverglass and a slide; thus a portion of the floating liposomes are out of focus. In all cases, an extensive clustering of liposomes was observed, suggesting that there is a net attraction between the lipid membranes in spite of the charges introduced via labeling. This is analogous to the interactions of neat DMPC membranes in the same temperature range [13]. While small liposomes appear fully illuminated without any discernible internal structure, the larger, well resolved structures are mostly hollow albeit with a wall thickness that suggests some degree of multilamellarity. Importantly, liposomes could be imaged for hours without a reduction in the luminescent intensity, demonstrating the high photochemical stability of the complexes.

In images of labeled DMPC membranes (Fig. 3), the luminescent intensity does not exhibit noticeable variations between or within the liposomes, thus both $[Ir(ppy)_2(dnbpy)]^{+}$ (Fig. 3 A, B) and

Table 1
Photophysical properties of the metallosurfactant species in different environments.

Complex	Solvent system	PL λ_{max}/nm	Quantum yield ϕ_p/%	Lifetime τ_p/ns
$[Ru(bpy)_2(dnbpy)]^{2+}$	Deoxygenated CH_3CN	628	56.4	888
	CH_3CN		0.9	147
	Liposome in PBS	655	2.7	368
$[Ir(ppy)_2(dnbpy)]^{+}$	Deoxygenated CH_3CN	586	23.1	555
	CH_3CN		2.6	63
	Liposome in PBS	600	8.4	610, 161, 70

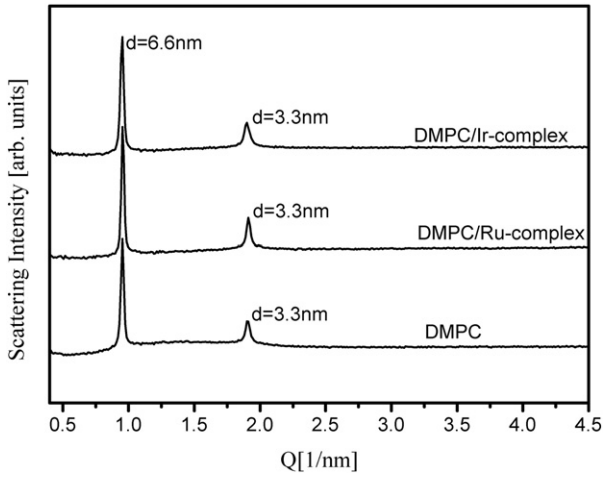

Fig. 3. Fluorescence microscopy images of giant DMPC liposomes labeled with: (A)–(B) $[Ir(ppy)_2(dn\text{-}bpy)]^+$ and (C)–(D): $[Ru(bpy)_2(dn\text{-}bpy)]^{2+}$. Images taken with (A)–(C) a wide field fluorescence microscope and (D) confocal fluorescence microscope. Images (A)–(C) were captured with the same magnification.

$[Ru(bpy)_2(dn\text{-}bpy)]^{2+}$ (Fig. 3 C, D) are evenly distributed in the membrane. Images of DMPC:DMPG 4:1 liposomes (Fig. S2) exhibit much weaker luminescent intensities with both labels than neat DMPC membrane, but with some background luminescence present in all images. Given that DMPC:DMPG 4:1 liposomes tend to be unilamellar, the amount of luminophore per liposome is necessarily less, while the direct access to oxygen in the buffer solution may cause partial quenching in this case. It is known that a large population of SUVs is also present even in the absence of any mechanical stimulation [47], thus the background signal is the result of moving small liposomes that are smaller than the diffraction limit and cannot be resolved optically, while their constant Brownian motion makes it impossible to capture them even as point sources in solution imaging. In the case of the $[Ir(ppy)_2(dnbpy)]^+$ label, the larger liposomes appear hollow but with bright spots, which could be small liposomes attached to the surface, or inhomogeneous label distribution. Nanoscale domain separation of DMPC:DMPG mixture was observed before [47] and thus it is possible that the label fractions between these domains. The liposomes containing 10% cholesterol (Fig. S3) are large, partially multilamellar and in their appearance they are very similar to liposomes of neat DMPC.

Control measurements were performed using "tailless" complexes: hydrophilic $[Ru(bpy)_3]^{2+}$ and hydrophobic $[Ru(dpp)_3]^{2+}$ (where dpp is 4,7 diphenyl phenanthroline). In the first case, as $[Ru(bpy)_3]^{2+}$ is not sufficiently soluble in chloroform to premix it with lipids, the complex was added to an aqueous liposome suspension. The phosphorescence of this complex is quenched by oxygen in the solution and it would only luminesce if incorporated into the membrane, thus the lack of any emission in the presence of liposomes confirmed that the hydrophilic analogue of the lipid-mimetic label does not incorporate into the membrane. The hydrophobic complex $[Ru(dpp)_3]^{2+}$ was soluble in organic solvents and thus it was possible to premix it with lipids, however upon hydration in aqueous buffer solution the mixture could not be dispersed and thus it did not form liposomes. These observations clearly demonstrate that the lipid-mimetic nature of the two compounds, that is, the hydrophobic domain of the two aliphatic chains and the compact hydrophilic head group are both required for successful membrane labeling.

Dynamic light scattering (DLS) measurements were performed to analyze the size distribution of the liposomes. The preparation method as described above produces a very broad, polydisperse size distribution, with polydispersity index (PDI) values typically in the range of 0.6–1.0. However, the samples produced this way include multilamellar and giant vesicles and thus the same preparations are suitable for SAXS, fluorescent microscopy and AFM, providing methodological coherence for the work.

To obtain quantitative information from DLS, Z-average values were determined from measurements with the lowest polydispersity values.

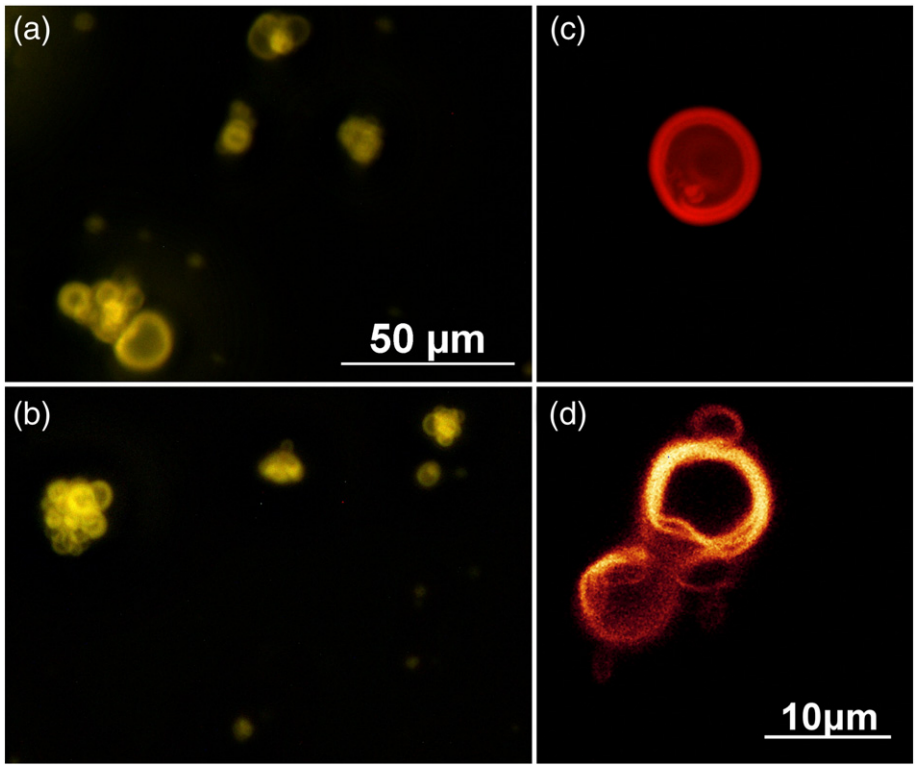

Fig. 4. SAXS patterns of $[Ru(bpy)_2(dn\text{-}bpy)]^{2+}$ labeled, $[Ir(ppy)_2(dn\text{-}bpy)]^+$ labeled and neat DMPC suspensions in phosphate buffer with 100 mM NaCl.

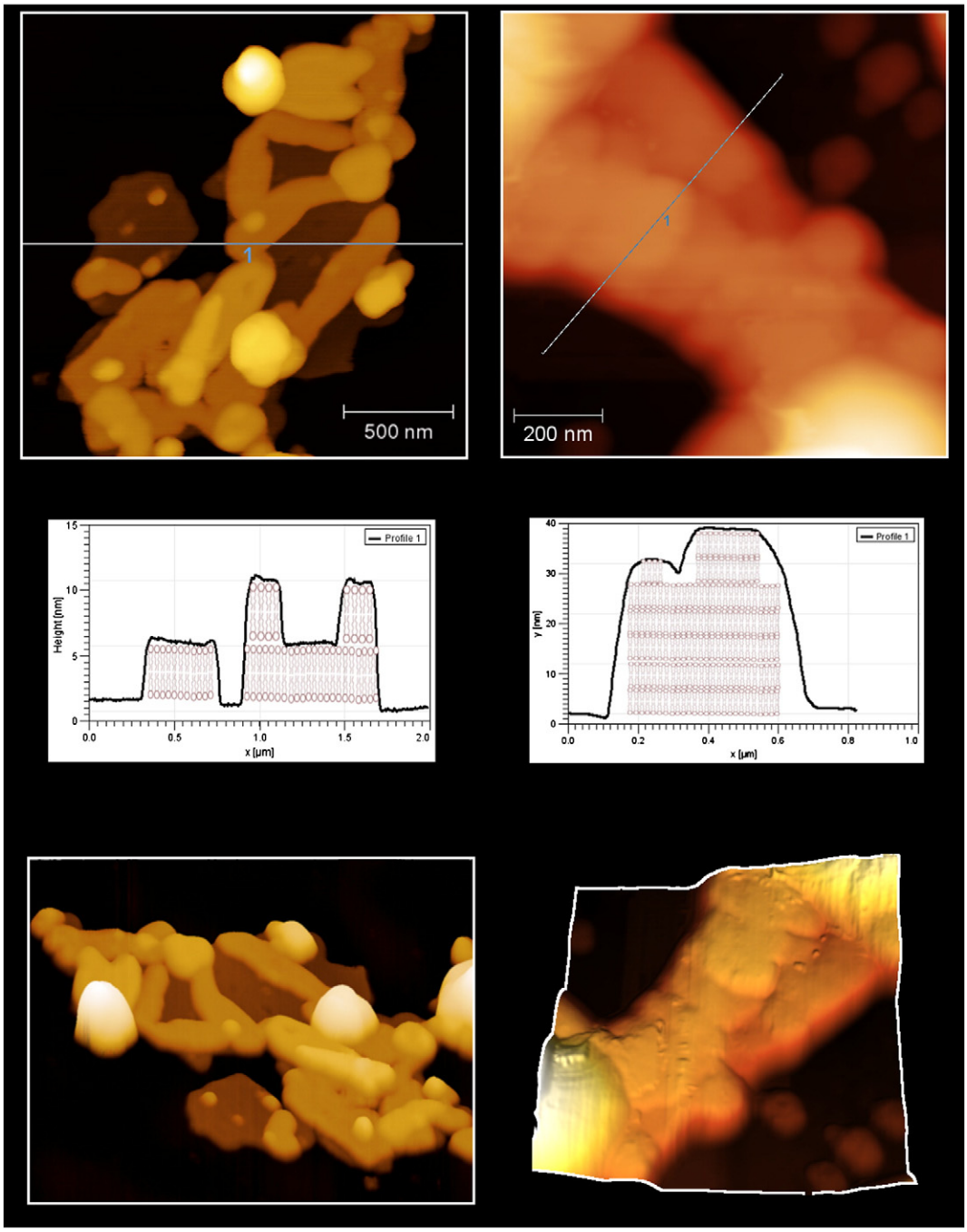

Fig. 5. AFM images of dry $[Ir(ppy)_2(dn\text{-}bpy)]^+$ and $[Ru(bpy)_2(dn\text{-}bpy)]^{2+}$ labeled DMPC membranes deposited on mica surface (left panels and right panels, respectively). From top to bottom: topography images; section profile along the lines in the topography images; three dimensional representation of the topography. In the section profiles, schematics of membrane bilayer stacking have been included to illustrate the internal structure.

For $[Ru(bpy)_2(dnbpy)]^{2+}$ the lowest PDI was 0.75 yielding Z_{avg} ~880 nm, and for $[Ir(ppy)_2(dnbpy)]^+$ labeled liposomes Z_{avg} of ~457 nm was obtained with PDI values of 0.6–0.7. For comparison, a neat DMPC suspension prepared and measured under the same conditions exhibited PDI values fluctuating in a range of 0.55–1.0 between measurements, yielding a broad range of Z-average diameters between 350 and 900 nm. The size distribution of liposomes is known to narrow over 20–30 h, or the process might be sped up using mechanical processes such as freeze-fracture or sonication [46]. In a previous work we found that upon aging neat DMPC suspensions a bimodal distribution emerges, containing a well defined population at a diameter of ~105 nm (SUV) and a broader, scattered population of larger liposomes in the 300–700 nm size range(EUV) [47] thus it is feasible to assume that the labeled liposomes follow this trend. To narrow the size distribution we used prolonged vortexing (~30 min) for the shear effect that is useful to separate liposome aggregates. As a result, PDI values have been reduced to the range of 0.2–0.3. Bimodal size distributions were resolved in both cases, with $[Ir(ppy)_2(dnbpy)]^+$ and $[Ru(bpy)_2(dnbpy)]^{2+}$ labeled liposomes exhibiting SUV populations at 38.9 nm and 111 nm, and EUV populations at 163 nm and 361 nm, respectively. Thus, the labeled liposomes follow the same trend and form in a similar size range to neat DMPC, with $[Ir(ppy)_2(dnbpy)]^+$ labeling resulting in smaller liposomes. Given that membrane bending modulus, and thus liposome size is a sensitive function of the ionic strength of the environment [46,48], the inclusion of the labels in the membrane may perturb the local ionic environment by reducing the

concentration of Na^+, leading to a slight variation in the membrane bending modulus. Importantly, in pure water the diameter of the smallest liposome population is reported to be ~20 nm [49] in light of which the effect of either of the complexes on the membrane bending modulus is negligible.

To test for any structural differences between neat and $[Ru(bpy)_2(dn\text{-}bpy)]^{2+}$ and $[Ir(ppy)_2(dn\text{-}bpy)]^+$ labeled membranes, synchrotron SAXS measurements were performed. Clear diffraction patterns were obtained with sharp Bragg's peaks, suggesting a high degree of multilamellarity (Fig. 4). The SAXS patterns collected for the liposomes containing $[Ru(bpy)_2(dn\text{-}bpy)]^{2+}$ or $[Ir(ppy)_2(dn\text{-}bpy)]^+$ were identical to those for neat DMPC liposomes. This confirms that the presence of the metal complexes does not induce any significant change in the biomembrane. In spite of the hollow appearance of the liposomes in Fig. 3, the sharp Bragg's peaks of the SAXS measurements reveal a substantial ordered crystalline size, that is, a high degree of multilamellarity. SAXS literature typically describes liposomes as multilayer vesicles based on classical surfactant self-assembly theory according to which only SUVs are stable and any larger structures have to be multilamellar structures with an SUV core [12,44,45]. Our results, however, suggest that the sharp diffraction peaks originate from hollow, large multilamellar liposomes that, with a bilayer stack thickness of only a few hundred nanometers, do not require geometric constraints of the innermost bilayer to be stable over time. Thus it is reasonable to conclude that the fluorescence microscopy images faithfully represent the structure and clustering of neat DMPC membranes.

DMPC liposomes have the ability to fuse into supported single- and multilamellar membranes if deposited onto a mica surface, which can be imaged with AFM [43]. At low surface coverage, islands of membrane might be created that allow for accurate height measurements, without the need for force dissection [51]. Since the ability to fuse is generally a function of the physical properties (surface tension, elasticity) of the membranes, changing the lipid composition may leave intact liposomes on the surface instead of a fused membrane [47]. Accordingly, imaging the deposits formed by the labeled liposomes is a good way of qualitatively assessing their physical properties in relation to neat DMPC membranes.

AFM images of the labeled membranes are shown in Fig. 5. The images reveal mostly flat lamellar geometries, characteristic of supported DMPC membranes, and also demonstrated by the cross section profiles measured along the lines indicated in the topography images (Fig. 5, middle panels) [47]. $[Ir(ppy)_2(dn\text{-}bpy)]^+$ labeled DMPC membrane forms single bilayer membranes with islands of a second bilayer on top of the first one (Fig. 5, left panels). Schematics are added within the profile to illustrate the structure of the membranes. The thickness of the bilayers was measured using the cross section profile and was found to be ~5 nm, which is the same as the thickness of dried neat DMPC membrane and consistent with the SAXS measurements of the hydrated membranes. The $[Ru(bpy)_2(dn\text{-}bpy)]^{2+}$ containing DMPC forms multilayered membranes, the height of the lower "terrace" is consistent with the thickness of 6 bilayers(Fig. 5 right panels). Schematics added in the cross section profile to illustrate the position of these bilayers. While the edges of the structures appear slightly rounded due to tip convolution, the flat surfaces confirm that these are fused membranes and not aggregated liposomes, as the gaps between round liposomes would be clearly visible in the images. This observation is consistent with the multilamellar nature of the liposomes imaged with fluorescence microscopy.

4. Conclusions

In this study two lipid-mimetic phosphorescent metal complexes, $[Ru(bpy)_2(dn\text{-}bpy)]^{2+}$ and $[Ir(ppy)_2(dn\text{-}bpy)]^+$, have been synthesized and their utility as labels for lipid bilayer structures demonstrated. Photophysical characterization reveals relatively high quantum yields and long excited state lifetimes for both complexes. These properties are sensitive to oxygen, but incorporation into lipid bilayers provides substantial protection from such quenching mechanisms. The lipid mimetic complexes have been successfully incorporated into dimyristoyl-phosphatidylcholine (DMPC) liposomes in 0.1–5% concentrations. At only 0.5 mol% the metal complexes provide ample luminescence intensity for wide field fluorescence microscopy imaging. Small Angle X-ray Scattering (SAXS) measurements confirmed that the bilayer structures of DMPC with and without $[Ru(bpy)_2(dn\text{-}bpy)]^{2+}$ or $[Ir(ppy)_2(dn\text{-}bpy)]^+$ DMPC are identical. AFM imaging confirmed that the labeled liposomes fuse into lamellar membranes on mica surface similar to neat DMPC. These results confirm that both complexes are sufficiently lipid-mimetic and that lipid-mimetic luminescent transition metal complexes offer a powerful new approach to imaging and biophysical characterization of lipid membranes.

Author contributions

The manuscript was written through contributions of all authors. All authors have given approval to the final version of the manuscript.

Acknowledgement

Conor Hogan acknowledges the Australian Research Council for financial support through (DP1094179 and LE120100213).

Appendix A. Supplementary data

Supplementary data to this article can be found online at http://dx.doi.org/10.1016/j.bbamem.2014.08.005.

References

[1] J.T. Groves, R. Parthasarathy, M.B. Forstner, Fluorescence imaging of membrane dynamics, Annu. Rev. Biomed. Eng. 10 (2008) 311–338.
[2] R.P. Haughland, Handbook of Fluorescent Probes and Research Chemicals, 9th edn Molecular Probes Inc., Eugene, 1996.
[3] M.G. Wootan, N.M. Bass, D.A. Bernlohr, J. Storch, Fatty acid binding sites of rodent adipocyte and heart fatty acid binding proteins: characterization using fluorescent fatty acids, Biochemistry 29 (40) (1990) 9305–9311.
[4] F.S. Abrams, A. Chattopadhyay, E. London, Determination of the location of fluorescent-probes attached to fatty-acids using parallax analysis of fluorescence quenching — effect of carboxyl ionization state and environment on depth, Biochemistry 31 (23) (1992) 5322–5327.
[5] A.K. Lala, V. Koppaka, Fluorenyl fatty acids as fluorescent probes for depth-dependent analysis of artificial and natural membranes, Biochemistry 31 (24) (1992) 5586–5593.
[6] H.J. Galla, E. Sackmann, Chemically induced phase separation in mixed vesicles containing phosphatidic acid. Optical study, J. Am. Chem. Soc. 97 (14) (1975) 4114–4120.
[7] T. Stegmann, P. Schoen, R. Bron, J. Wey, I. Bartoldus, A. Ortiz, J.L. Nieva, J. Wilschut, Evaluation of viral membrane fusion assays. Comparison of the octadecylrhodamine dequenching assay with the pyrene excimer assay, Biochemistry 32 (42) (1993) 11330–11337.
[8] V. Fernandez-Moreira, F.L. Thorp-Greenwood, M.P. Coogan, Application of d(6) transition metal complexes in fluorescence cell imaging, Chem. Commun. 46 (2) (2010) 186–202.
[9] A.J. Amoroso, M.P. Coogan, J.E. Dunne, V. Fernandez-Moreira, J.B. Hess, A.J. Hayes, D. Lloyd, C. Millet, S.J.A. Pope, C. Williams, Rhenium fac tricarbonyl bisimine complexes: biologically useful fluorochromes for cell imaging applications, Chem. Commun. 29 (2007) 3066–3068.
[10] S.W. Hell, Far-field optical nanoscopy, Science 316 (2007) 1153–1158.
[11] Z. Chen, V.W. Cornish, W. Min, Chemical tags: inspiration for advanced imaging techniques, Curr. Opin. Chem. Biol. 17 (4) (2013) 637–643 (Published: AUG 2013).
[12] J.N. Israelachvili, D.J. Mitchell, B.W. Ninham, Theory of self-assembly of hydrocarbon amphiphiles into micelles and bilayers, J. Chem Soc. Faraday Trans. 2 72 (1976) 1525–1568.
[13] J.N. Israelachvili, Intermolecular and Surface Forces, revised third edition Academic press, 2011.
[14] J. Pan, T.T. Mills, S. Tristram-Nagle, J.F. Nagle, Cholesterol perturbs lipid bilayers nonuniversally, Phys. Rev. Lett. 100 (2008) (Art no.198103).
[15] O. Maier, V. Oberle, D. Hoekstra, Fluorescent lipid probes: some properties and applications (a review), Chem. Phys. Lipids 116 (1–2) (2002) 3–18.

[16] R.A. Parente, B.R. Lentz, Advantages and limitations of 1-palmitoyl-2-[[2-[4-(6-phenyl-trans-1,3,5-hexatrienyl)phenyl]ethyl]carbonyl]-3-sn-phosphatidylcholine as a fluorescent membrane probe, Biochemistry 24 (22) (1985) 6178–6185.
[17] L.M.S. Loura, F. Fernandes, A.C. Fernandes, J.P.P. Ramalho, Effects of fluorescent probe NBD-PC on the structure, dynamics and phase transition of DPPC. A molecular dynamics and differential scanning calorimetry study, Biochim. Biophys. Acta Biomembr. 1778 (2) (2008) 491–501.
[18] P.J. Somerharju, J.A. Virtanen, K.K. Eklund, P. Vainio, P.K.J. Kinnunen, 1-Palmitoyl-2-pyrenedecanoyl glycerophospholipids as membrane probes: evidence for regular distribution in liquid-crystalline phosphatidylcholine bilayers, Biochemistry 24 (11) (1985) 2773–2781.
[19] S. Ohki, T.D. Flanagan, D. Hoekstra, Probe transfer with and without membrane fusion in a fluorescence fusion assay, Biochemistry 37 (20) (1998) 7496–7503.
[20] R.G. Ashcroft, K.R. Thulborn, J.R. Smith, H.G.L. Coster, W.H. Sawyer, Perturbations to lipid bilayers by spectroscopic probes as determined by dielectric measurements, Biochim. Biophys. Acta 602 (2) (1980) 299–308.
[21] J. Lakowicz, Principles of Fluorescence Spectroscopy, Springer, New York, 2006.
[22] G.A. Reitz, J.N. Demas, B.A. Degraff, E.M. Stephens, Inter- and intramolecular excited-state interactions of surfactant-active rhenium(I) photosensitizers, J. Am. Chem. Soc. 110 (15) (1988) 5051–5059.
[23] L.A. Sacksteder, M. Lee, J.N. Demas, B.A. Degraff, Long-lived, highly luminescent rhenium(I) complexes as molecular probes: intra- and intermolecular excited-state interactions, J. Am. Chem. Soc. 115 (18) (1993) 8230–8238.
[24] M.S. Lowry, W.R. Hudson, R.A. Pascal, S. Bernhard, Accelerated luminophore discovery through combinatorial synthesis, J. Am. Chem. Soc. 126 (43) (2004) 14129–14135.
[25] D.J. Stufkens, A. Vlcek, Ligand-dependent excited state behaviour of Re(I) and Ru(II) carbonyl-diimine complexes, Coord. Chem. Rev. 177 (1998) 127–179.
[26] N.P. Cook, V. Torres, D. Jain, A.A. Marti, Sensing amyloid-beta aggregation using luminescent dipyridophenazine ruthenium(II) complexes, J. Am. Chem. Soc. 133 (29) (2011) 11121–11123.
[27] K.W. Huang, A.A. Marti, Recent trends in molecular beacon design and applications, Anal. Bioanal. Chem. 402 (10) (2012) 3091–3102.
[28] A. Indapurkar, B. Henriksen, J. Tolman, J. Fletcher, Evaluation of triazole-chelated lanthanides as chemically stabile bioimaging agents, J. Pharm. Sci. 102 (8) (2013) 2589–2598.
[29] R. Zhang, Z.Q. Ye, B. Song, Z.C. Dai, X. An, J.L. Yuan, Development of a ruthenium(II) complex-based luminescent probe for hypochlorous acid in living cells, Inorg. Chem. 52 (18) (2013) 10325–10331.
[30] S. Bonnet, B. Limburg, J.D. Meeldijk, R. Gebbink, J.A. Killian, Ruthenium-decorated lipid vesicles: light-induced release of Ru(terpy)(bpy)(OH2) (2+) and thermal back coordination, J. Am. Chem. Soc. 133 (2) (2011) 252–261.
[31] F.R. Svensson, M. Li, B. Nordén, P. Lincoln, Luminescent dipyridophenazine-ruthenium probes for liposome membranes, J. Phys. Chem. B 112 (35) (2008) 10969–10975.
[32] K.K.W. Lo, P.K. Lee, J.S.Y. Lau, Synthesis, characterization, and properties of luminescent organoiridium(III) polypyridine complexes appended with an alkyl chain and their interactions with lipid bilayers, surfactants, and living cells, Organometallics 27 (13) (2008) 2998–3006.
[33] L. Li, H. Szmacinski, J.R. Lakowicz, Long-lifetime lipid probe containing a luminescent metal-ligand complex, Biospectroscopy 3 (2) (1997) 155–159.
[34] L. Li, H. Szmacinski, J.R. Lakowicz, Synthesis and luminescence spectral characterization of long-lifetime lipid metal-ligand probes, Anal. Biochem. 244 (1) (1997) 80–85.
[35] F.M. el Torki, R.H. Schmehl, W.F. Reed, Photoinduced electron-transfer reactions of micelle-forming surfactant ruthenium(II) bipyridyl derivatives, J. Chem. Soc., Faraday Trans. 1 85 (2) (1989) 349–362.
[36] A. Guerrero-Martınez, Y. Vida, D. Domınguez-Gutierrez, R.Q. Albuquerque, L. De Cola, Tuning emission properties of iridium and ruthenium metallosurfactants in micellar systems, Inorg. Chem. 47 (2008) 9131–9133.
[37] G.J. Barbante, C.F. Hogan, D.J.D. Wilson, N.A. Lewcenko, F.M. Pfeffer, N.W. Barnett, P.S. Francis, Simultaneous control of spectroscopic and electrochemical properties in functionalised electrochemiluminescent tris(2,2′-bipyridine)ruthenium(II) complexes, Analyst 136 (7) (2011) 1329–1338.
[38] D.J.E. Piper, G.J. Barbante, N. Brack, P.J. Pigram, C.F. Hogan, Highly stable ECL active films formed by the electrografting of a diazotized ruthenium complex generated in situ from the amine, Langmuir 27 (1) (2011) 474–480.
[39] R.V. Kiran, C.F. Hogan, B.D. James, D.J.D. Wilson, Photophysical and electrochemical properties of phenanthroline-based bis-cyclometallated iridium complexes in aqueous and organic media, Eur. J. Inorg. Chem. 31 (2011) 4816–4825.
[40] S. Sprouse, K.A. King, P.J. Spellane, R.J. Watts, Photophysical effects of metal-carbon sigma bonds in ortho-metalated complexes of Ir(III) and Rh(III), J. Am. Chem. Soc. 106 (22) (1984) 6647–6653.
[41] K. Suzuki, A. Kobayashi, S. Kaneko, K. Takehira, T. Yoshihara, H. Ishida, Y. Shiina, S. Oishi, S. Tobita, Reevaluation of absolute luminescence quantum yields of standard solutions using a spectrometer with an integrating sphere and a back-thinned CCD detector, Phys. Chem. Chem. Phys. 11 (42) (2009) 9850–9860.
[42] A. Juris, V. Balzani, F. Barigelletti, S. Campagna, P. Belser, A. von Zelewsky, Ru(II) polypyridine complexes: photophysics, photochemistry, eletrochemistry, and chemiluminescence, Coord. Chem. Rev. 84 (1988) 85–277.
[43] R.P. Richter, R. Bérat, A.R. Brisson, Formation of solid-supported lipid bilayers: an integrated view, Langmuir 22 (8) (2006) 3497–3505.
[44] J. Valério, M.H. Lameiro, S.S. Funari, M.J. Moreno, E. Melo, Temperature effect on the bilayer stacking in multilamellar lipid vesicles, J. Phys. Chem. B 116 (1) (2011) 168–178.
[45] G. Pabst, J. Katsaras, V.A. Raghunathan, M. Rappolt, Structure and interactions in the anomalous swelling regime of phospholipid bilayers, Langmuir 19 (5) (2003) 1716–1722.
[46] M.M.A.E. Claessens, B.F. van Oort, F.A.M. Leermakers, F.A. Hoekstra, M.A.C. Stuart, Charged lipid vesicles: effects of salts on bending rigidity, stability, and size, Biophys. J. 87 (6) (2004) 3882–3893.
[47] A. Mechler, S. Praporski, S. Piantavigna, S.M. Heaton, K.N. Hall, M.-I. Aguilar, L.L. Martin, Structure and homogeneity of pseudo-physiological phospholipid bilayers and their deposition characteristics on carboxylic acid terminated self-assembled monolayers, Biomaterials 30 (4) (2009) 682–689.
[48] M.M.A.E. Claessens, F.A.M. Leermakers, F.A. Hoekstra, M.A.C. Stuart, Opposing effects of cation binding and hydration on the bending rigidity of anionic lipid bilayers, J. Phys. Chem. B 111 (25) (2007) 7127–7132.
[49] B.A. Cornell, G.C. Fletcher, J. Middlehurst, F. Separovic, The lower limit to the size of small sonicated phospholipid-vesicles, Biochim. Biophys. Acta 690 (1) (1982) 15–19.
[50] M.P. Del Borgo, A.I. Mechler, D. Traore, C. Forsyth, J.A. Wilce, M.C.J. Wilce, M.-I. Aguilar, P. Perlmutter, Supramolecular self-assembly of N-acetyl capped β-peptides leads to nano-to macroscale fibre formation, Angew. Chem. Int. Ed. 52 (32) (2013) 8266–8270.
[51] J. Thimm, A. Mechler, H. Lin, S. Rhee, R. Lal, Calcium-dependent open/closed conformations and interfacial energy maps of reconstituted hemichannels, J. Biol. Chem. 280 (11) (2005) 10646–10654.